Applied Catalysis B: Environment and Energy 344 (2024) 123625

Contents lists available at ScienceDirect

Applied Catalysis B: Environment and Energy

journal homepage: www.elsevier.com/locate/apcatb

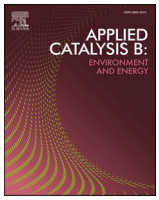

Smart and responsive zeolite catalysts for toluene "storage-oxidation" cycling removal

Lanlan Zhang [a,1], Zhihui Wang [a,1], Danyu Liu [a], Zelong Hao [a], Qi Zhao [b], Bingbing Chen [a,*], Chuan Shi [a,*]

[a] School of Chemistry, State Key Laboratory of Fine Chemicals, Dalian University of Technology, Dalian 116024, China
[b] Faculty of Chemistry and Chemical Engineering, Liaoning Normal University, Dalian 110629, China

ARTICLE INFO

Keywords:
Toluene
β zeolite
Storage and oxidation
Cu and Ag

ABSTRACT

"Storage - oxidation" cycling provides a novel and efficient route for VOCs' removal. Herein, Cu and Ag modified β zeolite with different SiO_2/Al_2O_3 ratio were prepared as smart and responsive materials for toluene removal. The storage strength for toluene on the metal sites (ion-exchange sites, metallic clusters and nanoparticles) and zeolite substrate (acid sites and channels) were discriminated, and the corresponding regeneration either by in-situ thermal oxidation or plasma assisted oxidation was coupled to fulfill the "storage-oxidation" cycle. By virtue of the collaboration of identified Cu^{2+} and Ag^{+} for toluene storage, a $Cu_{2.0}Ag_{3.0}$/β-25 catalyst was designed with high storage capacity (0.41 mmol/g) and adequate strength for trapping toluene, being available for in-situ thermal regeneration. In this study, the location of Cu and Ag species in β zeolite has been modulated to enable such smart and responsive materials available for toluene "storage and in-situ oxidation" cycling, which provides a general guidance for BTEX elimination.

1. Introduction

Volatile organic compounds (VOCs) are one of major air pollutants due to their toxicity and contribution for the formation of secondary pollutants, such as tropospheric ozone, PM2.5 and photochemical smog, which has attracted much concern regarding their impact on human health and general well-being [1–3].

Among various VOCs removal approaches, adsorption as an easy-operation and high-flexibility pathway, has been found in many applications in removing variety of VOCs, such as formaldehyde, benzene, toluene and so on [4]. Adsorption materials, including activated carbon, zeolite, and MOF have been thoroughly investigated, but the studies are mostly based on the material's physical properties such as pore structure and surface area [5–11]. In this regard, apart from high VOC adsorption capacity, efficient regeneration of the VOCs saturated materials without transfer gas pollutants to solid waste is also the important prerequisites for its practical application [7,12,13]. Accordingly, it is highly desirable to in-situ regenerate the saturated material, as well as establish an adsorption and in-situ regeneration cycled process for VOCs removal.

Thus, combining storage for low concentration VOCs capture followed by "in-situ" regeneration constitutes an effective and practical approach for low concentration indoor VOCs removal [14–19]. A dual functional catalyst was employed in this cycled process, which not only adsorbed VOCs molecules during the "storage" phase, but also in-situ oxidized the enriched VOCs into CO_2 and H_2O to regenerate the catalysts, subsequently the recovered material was ready for another storage regeneration cycle. The key issue to fulfilling such a cycle is to ensure no secondary pollutants production caused by the release of VOCs during regeneration, which requires the rate of VOCs oxidation is faster than that of VOCs desorption. In fact, it is quite tough to tackle this issue, since the affinity between VOCs and adsorbents is generally not strong enough to bind VOCs until the "light-off" temperature for catalytic oxidation [20]. Hence, how to strengthen the bonding between the target VOCs molecules and the adsorbents, and simultaneously accelerate the regeneration rate is still full of challenging [7].

As studied in our previous publications, HCHO was readily oxidized into formate species over transition metal oxide (Ag/Mn-CeO_x and Co-MnO_x et al.) catalysts [19,21]. Since it is a chemical reaction between HCHO and the adsorbents, there is no release of HCHO molecules during thermal regeneration, and an HCHO "storage-thermal oxidation" cycled

* Corresponding authors.
E-mail addresses: chenbb@dlut.edu.cn (B. Chen), chuanshi@dlut.edu.cn (C. Shi).
[1] These authors contributed equally.

https://doi.org/10.1016/j.apcatb.2023.123625
Received 3 September 2023; Received in revised form 16 November 2023; Accepted 6 December 2023
Available online 19 December 2023

process was established. While for benzene molecules, which are quite stable and hard to be oxidized at room temperature, a ZSM-5 or TS-1 zeolite was chosen to enrich low concentration benzene [14,15,17]. Since the interaction is mainly physical adsorption, it is inevitable that benzene is released before its thermal oxidation. Therefore, a cold plasma was employed to accelerate the rate for oxidation to establish a "storage-plasma regeneration" cycled process for benzene [22–25]. While there still remains a great challenge to fulfill a "storage-thermal regeneration" cycle for BTEX (referring to benzene, toluene, ethylbenzene and xylene) removal, especially when plasma is not recommended to use in some cases.

Herein, Cu and Ag modified β zeolite with $SiO_2/Al_2O_3 = 25$ and 300 were prepared as smart (represents for the identification of storage sites) and responsive (refers to adjusting the regeneration approach and executing the cycle) materials for "storage and in-situ oxidation" cycled removal of toluene. The location and nucleation of Cu and Ag species were identified by UV–vis, H_2-TPR and TEM characterizations. The storage capacity and strength for toluene adsorption on these metal (Cu or Ag) sites and zeolites were discriminated and correlated with the desorption behaviors. It is noticed that toluene could preferentially adsorb on the metal ions located at ion-exchange sites, which was partially oxidized to alkoxide. This strong bonding provides extended temperature window for toluene in-situ thermal oxidation before its release, and making the "storage-thermal regeneration" cycle feasible. On the other hand, if toluene is mostly adsorbed on the channel of hydrophobic β zeolite (SiO_2/Al_2O_3 =300), it is inevitable for the release of the physically adsorbed toluene during thermal oxidation, and a fast oxidation technique of cold plasma was introduced to realize the in-situ regeneration. The study presents a smart process of "Identification of storage sites - Adjusting regeneration approach - Executing the cycle" for toluene removal, which provides a general guidance for BTEX removal.

2. Experimental

2.1. Catalyst preparation

Cu and Ag-based catalysts with different metal contents were prepared by incipient wetness impregnation (IWI) method with a solution of $Cu(NO_3)_2$ or $AgNO_3$ at a constant temperature. Before contact with the substrate, the desired amount of $Cu(NO_3)_2$ or $AgNO_3$ was dissolved in needed deionized water. After impregnation, the sample was aged at room temperature for 12 h, followed by desiccation at 65 °C for 2 h in vacuum drying oven and then calcined in a muffle furnace at 450 °C for 4 h. The obtained catalysts were denoted as $Cu_x/β$-y or $Ag_x/β$-y (where x indicates the mass fraction of Cu/Ag; i.e., x%=1, 2, 3, 5%, y indicates the SiO_2/Al_2O_3 ratio of β zeolite; i.e., y = 25, 300).

The bimetallic $Cu_{2.0}Ag/β$-25 materials with different Ag contents were firstly prepared by the co-impregnation method. In a typical synthesis procedure, desired amount of $AgNO_3$ and $Cu(NO_3)_2$ were co-dissolved in a certain amount of deionized water. Then, the mixed solution was added dropwise to the β-25 zeolite. The impregnated samples were aged overnight at ambient temperature in darkness followed by dehydration at 65 °C for 2 h in vacuum drying oven and calcined in air at 450 °C for 4 h. These catalysts were labeled as $Cu_{2.0}Ag_m/β$-25 (where m indicates the mass fraction of Ag; i.e., m%=1, 3, 5%).

CuAg bimetallic catalysts were also prepared by the sequential wetness impregnation. For example, β-25 was impregnated with solution of silver nitrate with a constant concentration of ca. 3%, followed by drying and calcination at 450 °C for 4 h, and subsequently impregnated with solution of copper nitrate according to the metal loading of 2.0%, followed by drying at 65 °C for 2 h, then calcined at 450 °C for 4 h. The obtained catalyst was denoted as $Ag_{3.0}$-$Cu_{2.0}/β$-25. By adjusting the dipping sequence in the same way, the $Cu_{2.0}$-$Ag_{3.0}/β$-25 catalyst was acquired.

2.2. Characterizations

X-ray diffraction (XRD) patterns were recorded on an XRD-6000 (Shimadzu, Kyoto, Japan) with Cu Kα radiation source (λ = 0.1542 nm), and operated at 30 kV and 30 mA. The step-scan was taken over the 2θ in the range of 10–50° with a scanning rate of 10 °/min. Crystallographic information was obtained by comparing the obtained XRD patterns to the Joint Committee on Powder Diffraction Standards (JCPDS).

Nitrogen adsorption-desorption was measured at −196 °C on Micromeritics ASAP 2460 analyzer. Prior to the measurement, all catalysts were degassed in vacuum at 200 °C for 4 h. The Brunauer-Emmett-Teller (BET) method was applied to calculate the total surface area (S_{BET}). The pore volume and pore size of them were also measured on the same instrument.

Transmission Electron Microscope (TEM) images were recorded on a Tecnai G2 F30 S-Twin system (Thermo Scientific, America) operated at 300 kV. Prior to the measurement, the catalyst was dispersed in absolute ethanol for 30 min under ultra-sonication condition and subsequently dripped on a copper grid.

Hydrogen temperature-programmed reduction (H_2-TPR) measurements were performed on a Micromeritics AutoChem II 2920 chemisorption analyzer. 0.16 g catalyst was loaded in a U-shape quartz reactor. The catalyst was purged at 300 °C for 60 min in Ar (30 mL/min), and then cooled down to 30 °C. Subsequently, the pretreated catalyst was heated from 30 to 800 °C in 5% H_2/Ar (100 mL/min) at a ramping rate of 10 °C/min.

UV–visible spectrum (UV–vis) was recorded in the range of 190–800 nm using a UV-550 spectrometer.

In-situ Drifts measurements were performed using a Bruker Tensor 27 spectrometer equipped with MCT detector. The sample was first pretreated at 400 °C for 30 min in N_2 flow and then cooled down to 30 °C. A background spectrum was recorded at 30 °C under N_2 flow. After the adsorption and purging steps, the temperature was raised for the desorption process. Drift spectra subtracted the background spectrum and were recorded accumulated for 60 scans with a resolution of 4 cm^{-1} at 30 °C under N_2 flow.

2.3. C_7H_8 Temperature-programmed desorption experiments

In a typical TPD experiment, the sample was first pretreated at 450 °C with a flowing N_2 (50 mL/min) for 1 h, and subsequently cooled down to room temperature. The flow was then switched to 25 ppm C_7H_8/21% O_2/RH= 50% (25 °C)/N_2 (100 mL/min in total) until the outlet toluene concentration reached 10% of the feed concentration. After purging the sample with N_2 (50 mL/min) for another 30 min to remove weakly adsorption reactants, the temperature was raised to 500 °C with a heating rate of 10 °C/min under a flowing N_2. The effluent gases were detected online using a mass spectrometer (Pfeiffer vacuum OmniStar™, GSD350).

2.4. Catalyst evaluation

The catalytic activity evaluations include two processes: the storage process and the in - situ regeneration process. Both were carried out in a continuous flow fixed bed quartz microreactor at atmospheric pressure. 65 mg catalyst (20–40 mesh) was placed in a fixed-bed quartz tubular micro-reactor with a diameter of 6 mm. Before performing the experiment, the catalysts were pretreated in the N_2 flow at 400 °C for 1 h. The storage process was carried out at room temperature, and 25 ppm C_7H_8/21% O_2/RH = 50% (25 °C)/N_2 was purged into the reactor at a continuous flow of 100 mL/min corresponding to a space velocity (SV) of 36,000 /h. Gaseous H_2O was carried into the gas stream by passing N_2 through a bubbler in a water bath at room temperature. The amount of water expressed as the relative humidity (RH) at 25 °C, was controlled by adjusting the flow rate of N_2, while keep the total flow rate unchanged.

In thermal regeneration, the same simulated air stream without toluene was switched into the reactor, with the temperature ramped to 500 °C at 10 °C/min and held there for 10 min. In plasma regeneration, air without toluene was switched to the catalyst packed DBD, with discharge at input power of 30 W.

In this work, it was not possible to monitor the C_7H_8 concentration directly by NDIR (S710) equipment due to the interfering effects of water. Therefore, C_7H_8 concentration during adsorption was measured by converting it to CO_2 in a homemade VOCs-to-CO_2 converter (CuO-MnO_2/Al_2O_3 catalyst) at 450 °C and determined by the amount of the CO_2 formation.

C_7H_8 storage capacities were determined at 25 °C. The examined parameters, C_7H_8 storage capacity (N_{C7H8}, mmol/g_{cat}), C_7H_8 conversion to CO_2 ($X_{C7H8\rightarrow CO_2}$, %) and carbon balance (*B*c, %) are defined as follows:

$$N_{C_7H_8} = \frac{C^{in}_{C_7H_8} F_1 t_1}{W_{cat.}}$$

$$X_{C_7H_8\rightarrow CO_2}\left(\%\right) = \frac{C^{out}_{CO_2}}{7 \times C^{in}_{C_7H_8}} \times 100\%$$

$$B_c = \frac{n^{produced}_{CO} + n^{produced}_{CO_2} + 7 \times n^{desorption}_{C_7H_8}}{7 \times n^{stored}_{C_7H_8}} \times 100\%$$

Where C^{in}_{C7H8} is the C_7H_8 concentration in the feed gas. F_1 is the total flow rate, t_1 is the breakthrough time and $W_{cat.}$ is the catalyst weight. Breakthrough time was defined as the time when outlet C_7H_8 concentration reached 10% of feed concentration.

The proportion of toluene desorption below 500 °C is defined as follows:

$$\alpha = \left(1 - \frac{n^{produced\ above\ 500\ °C}_{COx}}{7 \times n^{stored}_{C_7H_8}}\right) \times 100\%$$

Where $n^{stored}_{C_7H_8} = C_{(C_7H_8)_s} F_1 t_1$, $C_{(C7H8)s}$ means C_7H_8 concentration in the feed gas during the storage phase; $n^{producedabove500°C}_{COx} = \int_0^{t_2} F_2 C_{CO} dt + \int_0^{t_2} F_2 C_{CO_2} dt$, C_{CO} and C_{CO2} are the concentrations of CO and CO_2 during the TPO-progress, F_1 and t_1 are the total flow rate and the breakthrough time, F_2 and t_2 are the oxidation period, respectively.

2.5. Density functional theory (DFT) calculations

The spin-polarized first-principle calculations are performed with Vienna Ab Initio Simulation Package (VASP) [26,27]. Perdew-Burke-Ernzerhof (PBE) functional was used to solve the Kohn-Sham equations within periodic boundary conditions [28]. The dispersion correction of the van der Waals interactions between adsorbates and catalysts, namely Cu(II) and Ag(I) substituted β-zeolites, partially charged Ag and CuO clusters in β-zeolite, and on (111) surfaces of Ag and CuO were handled with DFT-D3 method of Grimme with zero-damping function adopted and extended by Grimme et al. [29,30]. PBE+U calculations with U-J of 7.0 eV were also performed for CuO related structures [31]. The electron-nucleus interactions are described using PAW pseudopotentials [32]. A planewave cutoff of 400 eV was used throughout this work. A Γ-only k-point grid was used to sampling the Brillion zone for the calculations on structure and properties related to β-zeolite, while a 9 × 9 × 9 k-point grid was used for bulk CuO and Ag after bench mark calculation. The convergence criterion for energy is 1×10^{-5} eV and that for ionic relaxation is 0.01 eV/Å. With the above setup, the calculated lattice parameters of β-zeolite are 12.66, 12.66 and 26.41 Å, respectively, that for bulk Ag is 4.09 Å and those for CuO were calculated as 4.69, 3.48 and 5.16 Å, respectively and β is 98.30° [33–35]. The adsorption of toluene was investigated with unit cell of β-zeolite, 4-layered (4 ×4) supercell of Ag(111) and a 4-layered (2 ×2) supercell of CuO(111), respectively. Vacuum layer of at least 15 Å was used in these surface slab models. The adsorption energy of toluene (E_{ad}) was calculated as the difference in energy between the and the sum of toluene and bare catalyst structures as: $E_{ad} = E_{Toluene+Cat} - E_{Toluene} - E_{Cat}$ where $E_{Toluene+Cat}$, $E_{Toluene}$ and E_{Cat} are the energy of toluene adsorption structure, gaseous toluene and catalyst of interest, respectively. (1 eV = 96 kJ/mol).

3. Cu/β for toluene "storage-oxidation" cycling

3.1. Identification of Cu nucleation over β zeolite

Two sets of β zeolite with SiO_2/Al_2O_3 ratio of 25 and 300, being characterized for their hydrophilic and hydrophobic properties, were selected to load Cu with 1 wt%, 2 wt% and 5 wt%, respectively. For XRD patterns shown in Fig. 1(a), only diffractions peaks of β zeolite can be observed, the characteristic reflections of CuO crystal were not detected [36]. As to UV–vis spectra shown in Fig. 1(b), much stronger bands due to isolated Cu^{2+} ions located in the cation-exchange sites of β zeolite (220 nm being assigned to the charge transfer of O^{2-} to isolated Cu^{2+} and 700–800 nm being attributed to $^2E_g \rightarrow {}^2T_{2\,g}$ transition of Cu^{2+} ions in an octahedral environment) were observed over Cu/β-25 series samples, being consistent with its lower SiO_2/Al_2O_3 ratio which provides more ion-exchanges sites for Cu^{2+} exchange [37–40]. Bands between 250 to 400 nm were attributed to Cu-O-Cu clusters [38]. By comparing the spectra of Cu/β-25 and Cu/β-300 samples, the contribution from isolated Cu^{2+} ions became less over Cu/β-300 series samples, being consistent with its deficient ion exchange sites. With the increased Cu loading, the CuO clusters aggregated into large CuO NPs, leading to the bands between 250–350 nm red-shifted [41,42]. The nucleation degree was also reflected in the reducibility of Cu^{2+} and CuO clusters (Fig. 1 (c)). Only a reduction peak centered at ca.450 °C appeared over $Cu_{1.0}$/β-25 and $Cu_{2.0}$/β-25 samples, being corresponded to the reduction of isolated Cu^{2+} into Cu^+ [43]. When Cu loading was enlarged to 5 wt%, the reduction peak can be observed at 270 °C, which was due to the reduction of CuO clusters. For Cu-based β-300 zeolite, the H_2 consumption caused by the reduction of due to isolated Cu^{2+} species was invisible, being consistent with its much less cation exchange sites. CuO clusters being reduced at 270 ℃ were predominant species over $Cu_{1.0}$/β-300 and $Cu_{2.0}$/β-300 samples [44]. When Cu loading reached 5 wt%, the separated peaks at 250 and 300 °C were observed, which could be ascribed to the sequent reduction of CuO clusters to Cu^+ and then to Cu^0. This suggests that CuO clusters further aggregate into large ones with increased Cu loading over β-300 zeolite. However, no obvious nanoparticles could be detected under the present magnification in TEM images (Fig. S1). From the foregoing, it is clear that lower SiO_2/Al_2O_3 ratio of β-25 provides more ion-exchange sites for Cu^{2+} and therefore renders a better dispersion of Cu.

3.2. Identification of storage and oxidation sites for toluene

Copper loaded β zeolite were studied for their storage capacity for toluene at room temperature with relative humidity of 50%, the results were shown in Fig. 2(a). For β-25 zeolite itself, it showed toluene storage capacity (TSC) of 0.19 mmol/g, which can be mainly ascribed to toluene adsorbed on Bronsted acid sites, which desorbed at ca. 200 °C (shown in Fig. 2(b)). Loading 1 wt% and 2 wt% Cu did not enhance the storage capacity obviously, but the desorption behavior changed a lot. Over $Cu_{2.0}$/β-25, the desorption of weakly bonded toluene can hardly be observed, and only 23% of stored toluene was released below 500 °C. Correlated to the characterization results, isolated Cu^{2+} ions were dominant species over $Cu_{2.0}$/β-25, it can be deduced that toluene strongly adsorbed on Cu^{2+}, which hardly desorbed below 500 °C. When Cu loading increased to 5 wt%, the storage capacity decreased by half, and toluene only released 1% below 500 °C. It seems that CuO clusters partially blocked the sites of Cu^{2+} and H^+, leading to the decreased

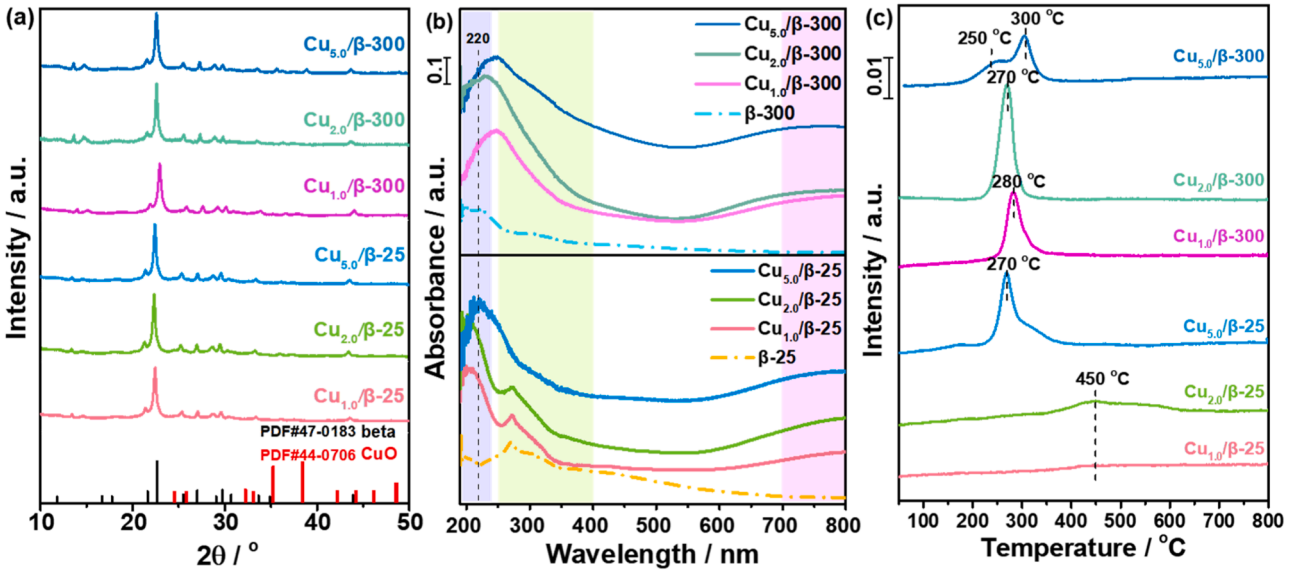

Fig. 1. Characterization of the Cu/β zeolites. (a) XRD patterns; (b) UV–vis spectra; (c) H_2-TPR profiles of the Cu/β-25 and Cu/β-300 series samples with different Cu contents.

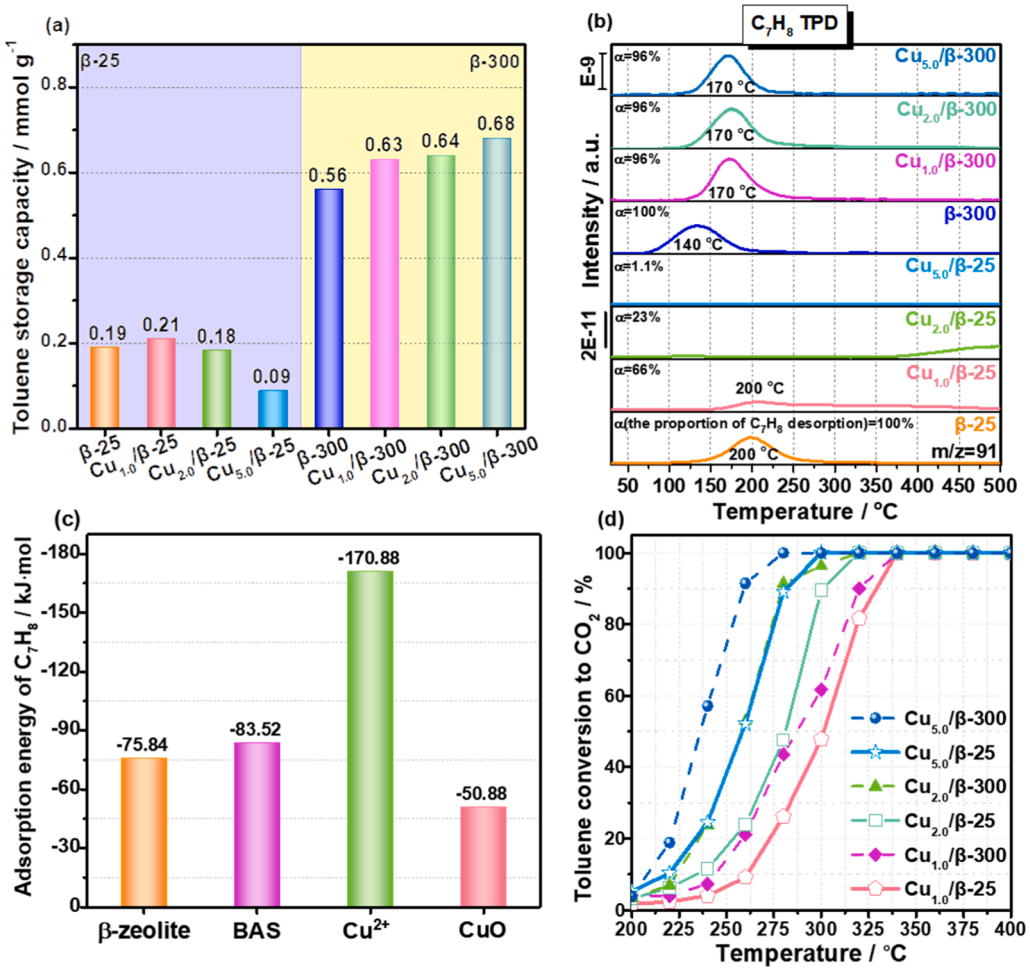

Fig. 2. (a) Toluene storage capacity of β-25, β-300 and Cu/β series zeolites under humid condition. Storage condition: 25 ppm C_7H_8 /21%O_2/N_2, RH= 50% (25 °C), F= 100 mL/min, GHSV= 36,000 /h; (b) Toluene TPD experiments over β-25, β-300 and Cu/β zeolites with different Cu loading. C_7H_8 - TPD condition: N_2, F= 100 mL/min, GHSV= 36,000 /h, 10 °C /min, 30–500 °C, The α represent the proportion of desorption toluene; (c) Calculated adsorption energy of toluene (E_{ad}); (d) The performance of toluene oxidation to CO_2 over Cu/β zeolites with different Cu loading. Oxidation condition: 25 ppm C_7H_8/21% O_2/N_2, RH= 50%(25 °C), F= 100 mL/min and GHSV = 36000 /h.

storage capacity. This was supported by N_2-physical adsorption results that the external surface area and micropore volumes declined with Cu loading (Table S1) [36]. For β-300 zeolite, it stored larger amount of toluene compared with β-25, which should be related to its hydrophobicity, but it desorbed mostly at lowest temperature of 140 °C. The result indicates hydrophobic channel could store more toluene, but the affinity is quite weak due to its physical adsorption nature (Fig. S2). The storage capacity increased with Cu loading slightly, but 96% of stored toluene was released below 200 °C. As CuO clusters are dominant species over Cu/β-300 samples, it is reasonable to deduce that toluene could adsorb on CuO clusters, but the strength is quite weak [45,46].

Such assignment is supported by the spin-polarized first-principle calculations shown in Fig. 2(c). The largest adsorption energy of toluene is linked with isolated Cu^{2+} (−170.88 kJ/mol), being in line with the observed partial oxidation of methyl into methoxyl [47]. Hydrogen bonding and pore-filling are the driving force for toluene adsorption on Bronsted sites and channel of β zeolite, so the interaction was much weaker, with adsorption energy of −83.52 kJ/mol and −75.84 kJ/mol, respectively. Due to the weak non-covalent interaction with benzene aromatic ring, CuO exhibited weakest adsorption affinity between toluene (−50.88 kJ/mol).

Compared Cu/β-25 and Cu/β-300 series samples, it is suggested that although zeolite with lower SiO_2/Al_2O_3 ratio with hydrophilic property possess lower toluene storage capacity due to H_2O occupying the channel of zeolite, the enriched cation sites provide more exchange sites for isolated Cu^{2+} sites, which strengthen toluene bonding and hardly release below 500 °C. While over hydrophobic zeolite with SiO_2/Al_2O_3 ratio of 300, the zeolite channel stores most of toluene molecules, but they are weakly bonded and easily desorbed. Moreover, CuO clusters render some additional weak sites for toluene adsorption.

The catalytic properties for toluene oxidation over Cu/β zeolite catalysts were compared and shown in Fig. 2(d). It seems that higher Cu loading (5 wt%) renders better catalytic performance, and there are no obvious impacts of SiO_2/Al_2O_3 ratio as 25 or 300 on the activity. The results indicate that aggregated CuO clusters play a key role in toluene oxidation, and higher than 99% conversion was obtained at 275 °C over $Cu_{5.0}$/β-300 and at 330 °C over $Cu_{5.0}$/β-25.

3.3. Unrevealing the stored toluene species

In-situ DRIFTs were conducted at 25 °C in the feed gas of 25 ppm C_7H_8/21%O_2/N_2, RH= 50% (25 °C) on $Cu_{2.0}$/β-25 and $Cu_{2.0}$/β-300 samples. The results were shown in Fig. 3. Over $Cu_{2.0}$/β-25 (Fig. 3 (a)), the broad band in the range of 3700–3100 cm^{-1} was ascribed to stretching mode of different types of hydroxyl groups (i.e. involved in hydrogen bonds), and the characteristic bands derived from the adsorbed toluene were detected at 3100–2800 (the stretching vibration of C-H groups) and 1376 cm^{-1} (the deformation of C-H bonding in -CH_3 group) [19,48]. It is noteworthy that the bands appeared at 1298 cm^{-1} and 1160 cm^{-1}, can be assigned to the CH_2 deformation vibration of benzyl species and C-O stretching vibration respectively, indicating the partial oxidation of toluene into benzyl alcohol over the $Cu_{2.0}$/β-25 catalyst [49,50]. During the desorption process in nitrogen, the peak at 1376 cm^{-1} was still visible when the temperature raised to 300 and 400 °C (Fig. S3). Meanwhile new bands at 1652 cm^{-1} and 1580 cm^{-1} appeared, which belonged to the benzaldehyde and asymmetric vibration (Vas(-COO)) of benzoic acid species, indicating the adsorbed benzyl alcohol was further oxidized to benzaldehyde and benzoic acid species with the increase of temperature [51,52]. In the case of $Cu_{2.0}$/β-300 sample (Fig. 3(b)), only bands at 1376 cm^{-1} ascribed to adsorbed toluene, ~3700–3100 cm^{-1} ascribed to hydroxyl groups and 1636 cm^{-1} attributed to molecular adsorbed H_2O could be observed, while toluene was the dominant specie at the end of the storage period [53]. Therefore, the results indicate that toluene was partially oxidized into benzyl alcohol during adsorption by isolated Cu^{2+} in the exchange site of β-25 zeolite, which explains its strong affinity with Cu/β-25. While only toluene molecules physically adsorbed on Cu/β-300, well explaining its weak interaction with Cu/β-300 samples.

3.4. Toluene removal by "storage-oxidation" cycling

One of key issues to fulfill such a "storage-oxidation" cycled removal is to avoid toluene release during in-situ oxidation regeneration. Considering the catalytic oxidation of toluene occurring at temperatures above 275 °C, the desorption below this temperature will result in

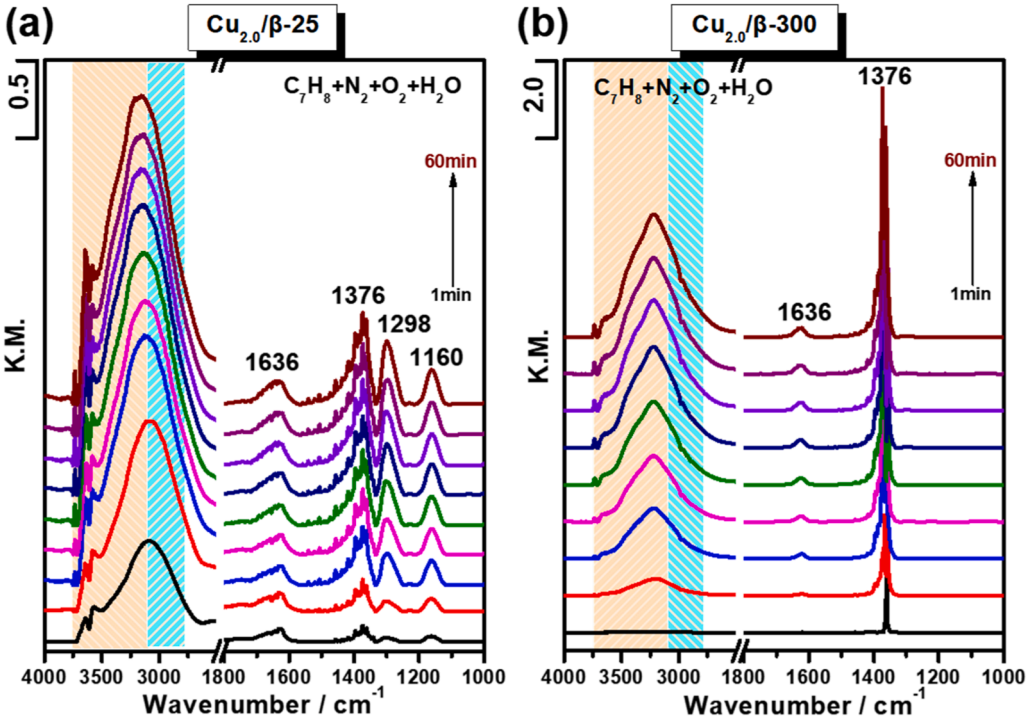

Fig. 3. In situ DRIFT spectra of toluene adsorption over (a) $Cu_{2.0}$/β-25 and (b) $Cu_{2.0}$/β-300 samples in the humid condition.

toluene release during regeneration. Obviously, $Cu_{1.0}$/β-25 and all the Cu/β-300 samples with low temperature desorption feature did not meet such requirement, and $Cu_{2.0}$/β-25 was selected to fulfill the "storage and in-situ thermal oxidation regeneration" cycling by virtue of its superior storage capacity and strength for toluene. As shown in Fig. 4(a), toluene was stored over the catalyst at room temperature in the presence of H_2O (RH=50%). During the regeneration phase, the stored toluene was completely oxidized into CO_x and H_2O at 324 °C without any release of toluene. The regenerated sample could store toluene again and fulfill another cycle, and the carbon balance for each cycle is over than 99%.

As to those weakly adsorbed toluene, such as those on $Cu_{2.0}$/β-300, it can be in-situ oxidized by cold plasma assisted oxidation. As shown in Fig. 4(b), the stored toluene could be totally oxidized with the assistance of plasma at room temperature without trace of toluene release. Such behavior is attributed to the fast reaction rate induced by cold plasma, which ensures the oxidation rate is faster than desorption rate to fulfill such a cycle [22]. And the conversion of stored toluene in the plasma regeneration was calculated to be over 99%, indicating its good regeneration ability.

4. Ag-β zeolite for toluene "storage-oxidation" cycling

4.1. Identification of Ag nucleation in β zeolite

Ag with 1 wt%, 3 wt% and 5 wt% loading on β zeolite with SiO_2/Al_2O_3 ratio of 25 and 300 were characterized by XRD, UV–vis and H_2-TPR respectively, and the results being shown in Fig. 5. As to XRD patterns (Fig. 5(a)), peaks attributed to β zeolite itself were clearly observed. Besides that, there was a peak at 38° ascribed to metallic Ag^0 over $Ag_{5.0}$/β-300 sample, indicating that Ag aggregated into

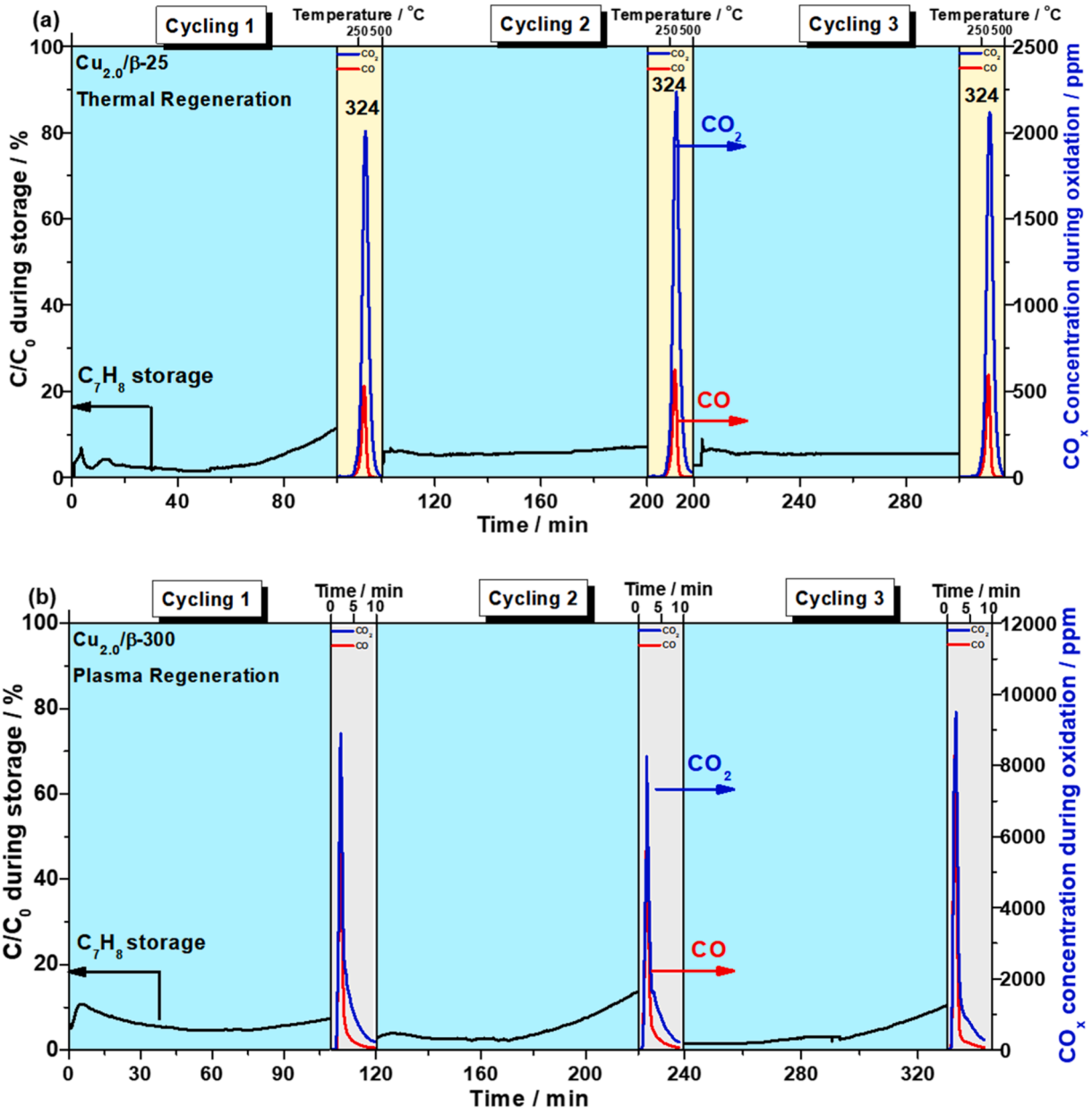

Fig. 4. (a) Toluene breakthrough curve (measured during storage phase) and CO_x concentration (measured during oxidation phase) during three consecutive "storage-thermal regeneration" cycles over $Cu_{2.0}$/β-25 zeolite. (b) Toluene breakthrough curve (measured during storage phase) and CO_x concentration (measured during oxidation phase) during three consecutive "storage-plasma regeneration" cycles over $Cu_{2.0}$/β-300 zeolite. Storage condition: 25 ppm C_7H_8 /21%O_2/N_2, RH= 50%(25 °C), F= 100 mL/min, GHSV= 36,000 /h; Oxidation condition: 21%O_2/N_2, RH= 50%(25 °C), F= 100 mL/min, GHSV= 36,000 /h, Heating rate= 10 °C/min or Input power= 30 W.

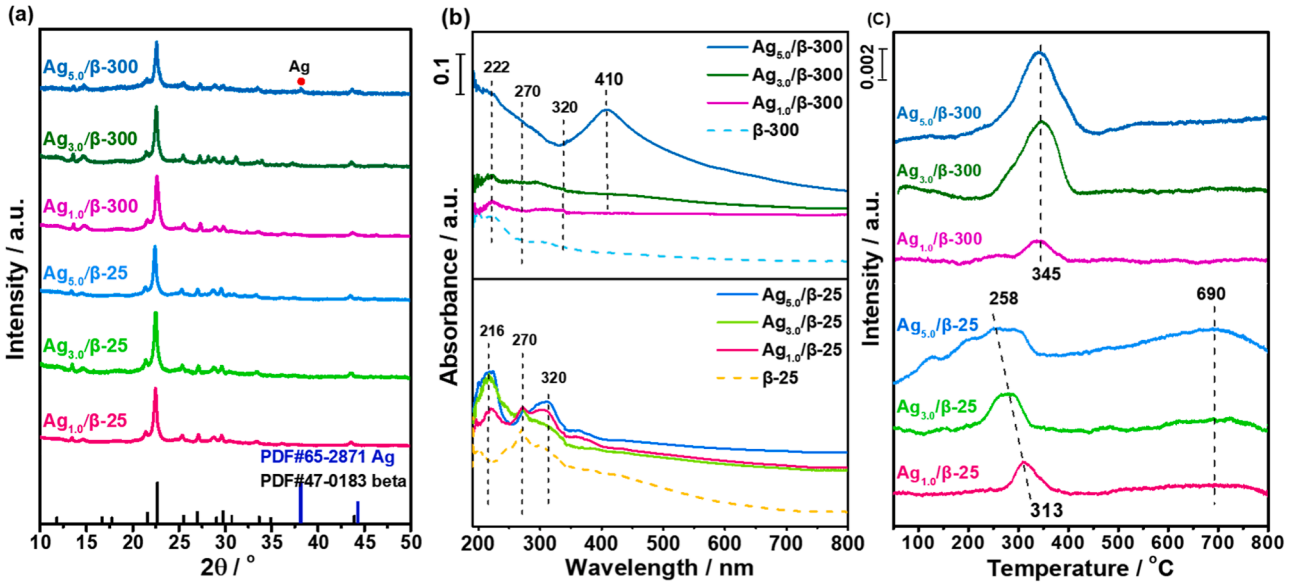

Fig. 5. Characterization of the Ag/β zeolites. (a) XRD patterns; (b) UV–vis spectra; (c) H_2-TPR of the Ag/β-25 and Ag/β-300 series samples with different Ag contents.

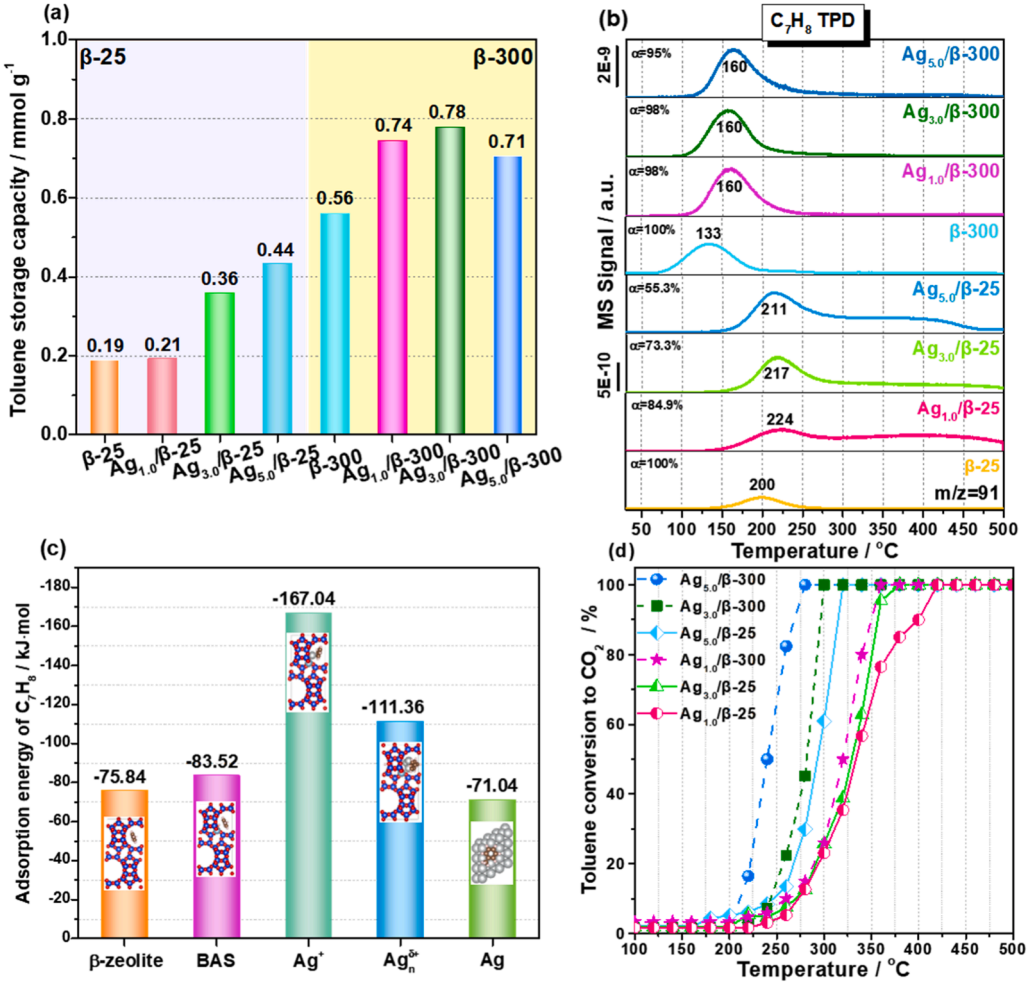

Fig. 6. (a) Toluene storage capacity of β-25, β-300 and Ag/β series zeolites under humid condition. Storage condition: 25 ppm C_7H_8/21%O_2/N_2, RH= 50% (25 °C), F= 100 mL/min, GHSV= 36,000 /h; (b) Toluene TPD experiments over β-25, β-300 and Ag/β zeolites with different Ag loading. C_7H_8 -TPD condition: N_2, F= 100 mL/min, GHSV= 36,000 /h, 10 °C /min, 30–500 °C, The α represent the proportion of toluene desorption; (c) Calculated adsorption energy of toluene (E_{ad}); (d) The performance of toluene oxidation to CO_2 over Ag/β zeolites with different Ag loading Oxidation condition: 25 ppm C_7H_8/21% O_2/N_2, RH= 50%(25 °C), F= 100 mL/min and GHSV = 36000 /h;.

nanoparticles when Ag loading was up to 5 wt% over β-300. For UV–vis (Fig. 5(b)), the absorption band at 216/222 nm was ascribed to the isolated Ag^+ on zeolite cation exchange sites and the bands at 270 and 320 nm were absorbance of charged $Ag_n^{\delta+}$ clusters located inside the zeolite channel [54,55]. While the broad band centered at 410 nm can be ascribed to the aggregated Ag nanoparticles located on the outer surface of zeolite [56]. For Ag/β-25 samples, Ag^+ and $Ag_n^{\delta+}$ clusters are dominant species, when Ag loading increased from 1 wt% to 5 wt%, the adsorption intensity enhanced accordingly. Comparatively, much less Ag^+ could be observed over Ag/β-300 catalyst, being consistent with its higher SiO_2/Al_2O_3 ratio. Along with Ag loading to 5 wt%, the nucleation of Ag increased greatly, leading to the formation of Ag nanoparticles, being in accordance with TEM results (Fig. S4).

As reflected in H_2-TPR (Fig. 5(c)), Ag^+ at the tion exchange site was difficult to reduce, which can only be clearly detected over $Ag_{5.0}$/β-25 at 690 °C owing to the highest proportion of Ag^+ as revealed by UV–vis results [57,58]. The overlapped and broad reduction peak ranging from 100 °C to 300 °C was ascribed to the reduction of $Ag_n^{\delta+}$ with various nucleation, and the largest H_2-consumption was obtained over-$Ag_{5.0}$/β-25, being consistent with its largest amount of charged silver clusters. When Ag was loaded on β-300 zeolite, the reduction peak due to isolated Ag^+ species is invisible, the reduction peak appeared at 345 °C, which was ascribed to the reduction of surface oxygen layer of Ag nanoparticles, corresponding to the adsorption band at 410 nm in UV–vis spectra.

4.2. Identify the sites for toluene storage and oxidation

As shown in Fig. 6(a), toluene storage capability of Ag/β samples at RT in the presence of moisture (RH=50% (25 °C)) were compared. $Ag_{1.0}$/β-25 possessed the similar storage capability with that of β-25 zeolite itself, but the desorption behavior showed big difference (Fig. 6 (b)). Besides the toluene desorption at 200 °C due to weakly adsorbed on Brønsted sites, a very broad and overlapped desorption ranging from 250 °C to 500 °C appeared over $Ag_{1.0}$/β-25, which should be ascribed to the desorption over $Ag_n^{\delta+}$ or isolated Ag^+ [50]. With increasing Ag loading to 5 wt%, the storage capability was doubled, and the corresponding desorption peaks between 250 °C-500 °C became stronger in intensity. It is noted that only ca. 55% of the stored toluene could be desorbed below 500 °C over $Ag_{5.0}$/β-25 sample, and obviously this value declined with Ag loading. Correlating with its enrichment in isolated Ag^+ species in $Ag_{5.0}$/β-25 sample, it is reasonable to deduce that toluene adsorption on Ag^+ is much stronger, which is hard to desorb even at 500 °C. The overlapped desorption between 250 °C-500 °C are mainly from $Ag_n^{\delta+}$ cluster, which is in line with their various nucleation numbers. Since Ag^+ represents the smallest nucleation, it is reasonable to deduce that the stronger affinity is formed over the smaller Ag clusters, which was supported by the DFT calculations that the largest adsorption energy of toluene was related to Ag^+ (−167.04 kJ/mol) and $Ag_4^{\delta+}$ (−111.36 kJ/mol), shown in Fig. 6(c).

For β-300 zeolite, due to its hydrophobic properties, toluene could be stored in the zeolite channel, and thereby showed great enhancement in toluene storage capability. The highest storage capacity of toluene was obtained over $Ag_{3.0}$/β-300 sample. The amount of stored toluene was enlarged along with the Ag loading, indicating that Ag could provide additional adsorption sites. Correlated with characterization results, the nano-sized silver particles can store toluene, but the affinity is quite weak, leading to the desorption at 160 °C [50]. This is in line with the DFT calculations that toluene adsorption energy of Ag NPs is the lowest (−71.04 kJ/mol).

This was also approved by in-situ DRIFT results of toluene adsorption in the stream of 25 ppm C_7H_8/21%O_2/RH= 50%/N_2, as shown in Fig. 7. Apart from the band at 1366 cm^{-1} (the deformation of C-H bonding of -CH_3 group) assigned to adsorbed toluene, the bands at 1292 and 1160 cm^{-1} attributed to the CH_2 deformation vibration of benzyl species and C-O stretching vibration were also observed, suggesting the formation of benzyl alcohol over $Ag_{5.0}$/β-25 sample (Fig. 7(a)) [58,59]. These bands were remained even the temperature rise to 300 or 400 °C, indicating a strong interaction between Ag^+ ions and the toluene molecule (Fig. S5) [58]. However, these partially oxidized species were

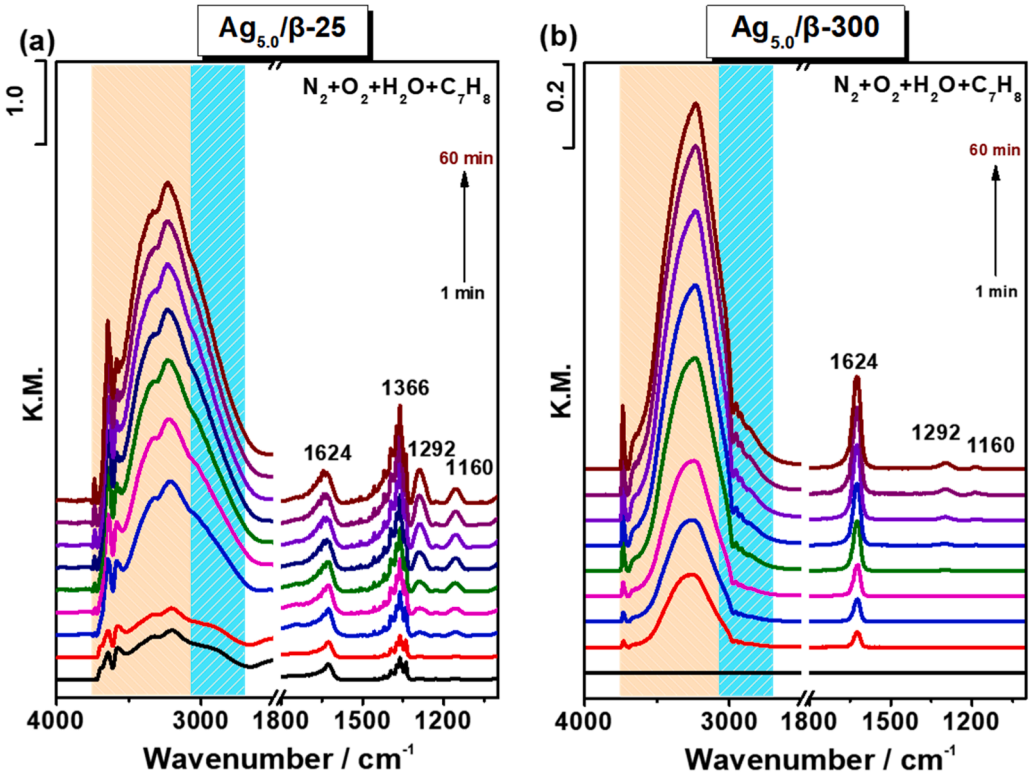

Fig. 7. In situ DRIFT spectra of toluene adsorption over (a) $Ag_{5.0}$/β-25 and (b) $Ag_{5.0}$/β-300 samples in the humid condition.

hardly observed over $Ag_{5.0}$/β-300 sample, on account of the physical adsorption of toluene on the sample. (The in-situ DRIFT results of toluene adsorption in the dry air were shown in Fig. S6).

The catalytic performance for toluene oxidation over Ag/β zeolite catalysts were shown in Fig. 6(d). The sample of 3 wt% and 5 wt% Ag loading on β-300 exhibited much higher activity than other samples, indicating that aggregated Ag nanoparticles play a key role in toluene oxidation.

4.3. Toluene removal by "storage-oxidation" cycle

As to the "storage-oxidation" cycle, since there is inevitable weakly adsorbed toluene over Ag NPs (which desorbed at 220 °C), while the oxidation requires temperature higher than 275 °C, it is unable to realize the in-situ thermal regeneration before its desorption. Accordingly, cold plasma assisted regeneration was employed here to enable the fast oxidation at room temperature. As shown in Fig. 8, the stored toluene in zeolite channel could be in-situ oxidized to CO_x and H_2O by plasma before it's desorption over $Ag_{5.0}$/β-300 sample, and the refreshed catalyst could be available for another cycle with carbon balance of over than 99% for each cycle.

5. Constructing efficient CuAg/β-25 catalyst for toluene "storage-oxidation" cycle

In the following section, we proposed a strategy of constructing Cu&Ag/β-25 catalyst by virtue of additional sites provided by $Ag_n^{\delta+}$ clusters to enhance the site density for chemical bonding of toluene, meanwhile in attempt to avoid the presence of silver nanoparticles that makes toluene weakly adsorbed. Cu and Ag were first co-impregnated onto β-25 to prepare the bi-metal exchanged β zeolites of $Cu_{2.0}Ag_{3.0}$/β-25 catalyst. Co-existence of Ag with Cu doping enhanced the toluene storage capacity obviously as shown in Fig. 9(a). At a certain Cu loading of 2 wt%, with increment of Ag loading from 1 to 3 wt%, the storage capacity doubled from 0.24 to 0.41 mmol/g. Significantly, there was no occurrence of toluene desorption ascribed to those on Ag NPs (at ca. 200 °C) (shown in Fig. 9(c)). But when Ag loading increased to 5 wt%, a peak assigned to toluene desorption at 307 °C appeared, indicating Ag aggregated when excessive Ag was introduced, generating weak bonding Ag centers for toluene.

The sequence of Cu and Ag doping was further optimized and the results are quite illustrative. It is noted worthy that the $Ag_{3.0}$-$Cu_{2.0}$/β-25 (loading Ag^+ first followed by Cu^{2+} sample), not only exhibited the higher storage capacity but no desorption of toluene below 300 °C, indicating that the improved storage strength and capacity towards toluene were simultaneously achieved. While for the reversed sequence of $Cu_{2.0}$-$Ag_{3.0}$/β-25 sample, a low temperature desorption of toluene featured at ca. 200 °C appeared, which has been ascribed to the weak affinity with Ag nanoparticles at the outer surface of zeolite, and the larger aggregated nanoparticles was evidenced in TEM images of Fig. 10 (a). These results suggest that the loading Ag^+ first followed by Cu^{2+} is preferred to avoid the severe aggregation of Ag. Combining the results of Cu and Ag co-impregnated sample, it is suggested that Ag^+ is much easier to occupy the exchange site in large membered rings than Cu^{2+} due to its larger ion radius [60–62]. Therefore, for the sample that Ag was firstly loaded or co-impregnated with Ag and Cu, Ag^+ preferentially occupied the ion exchange sites in large membered rings and rendered the better dispersion, as shown in Fig. 10(c). Furthermore, Cu^{2+} might inhibit the silver migration during calcination in assistant to avoid the presence of silver nanoparticles, resulting in increased amount of $Ag_n^{\delta+}$ clusters, thereby enhancing the storage capacity and adsorption strength of toluene [61,63,64].

Being consistent with above results, nanosized metallic particles show better catalytic oxidation ability (Fig. 9(b)), toluene could be totally oxidized into CO_2 and H_2O at 275 °C over $Cu_{2.0}$-$Ag_{3.0}$/β-25 catalyst.

Through optimizing the content and sequence for Ag introduction, not only enhanced the storage capacity compared with monometallic Cu sample, but also prevented the weakly interaction sites of Ag NPs generating over $Cu_{2.0}Ag_{3.0}$/β-25 catalyst. Thereby, in-situ thermal regeneration could be fulfilled over the $Cu_{2.0}Ag_{3.0}$/β-25 catalyst. As shown in Fig. 11, toluene was stored at room temperature for 240 min, and then being regenerated by in-situ heating the catalyst to 344 °C, and there was no release of toluene during regeneration. During 12 times cycles, the superior carbon balance of over than 98% was achieved, implying its good storage and regeneration ability.

The UV–vis and XPS characterizations were performed to investigate the surface state changes over $Cu_{2.0}Ag_{3.0}$/β-25 after the 12 times cycling reaction. As shown in Fig. S7 (a) and (b), the binding energy of Cu and Ag was similar for the fresh and used samples, indicated the surface

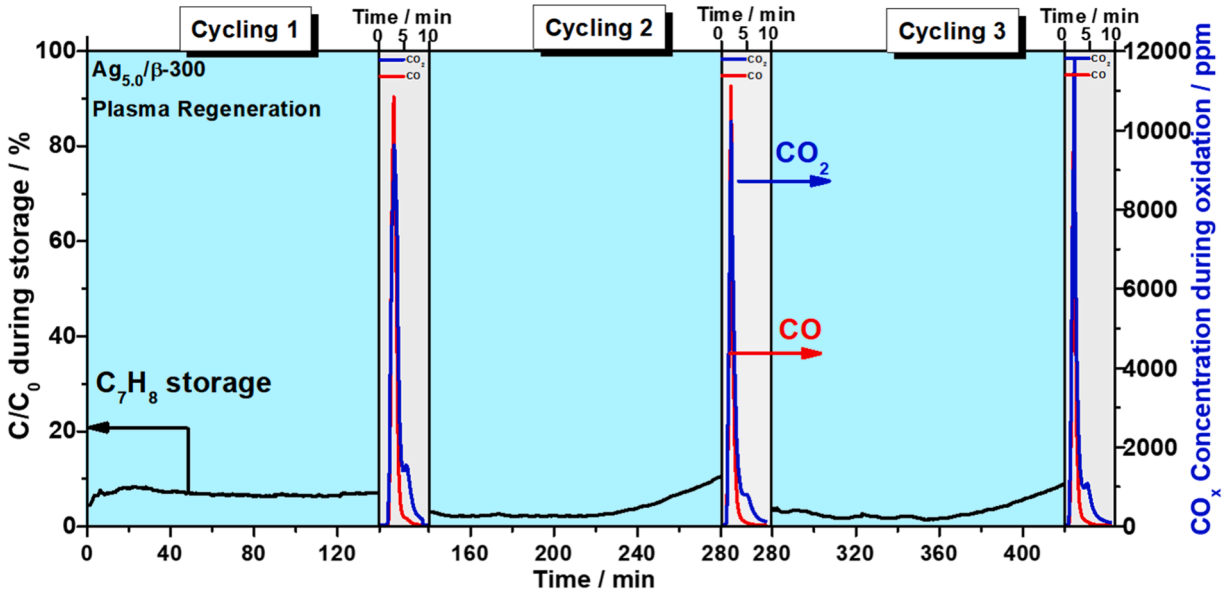

Fig. 8. Toluene breakthrough curve (measured during storage phase) and CO_x concentration (measured during oxidation phase) during three consecutive "storage-plasma regeneration" cycles over $Ag_{5.0}$/β-300 zeolite. Storage condition: 25 ppm C_7H_8 /21%O_2/N_2, RH= 50%(25 °C), F= 100 mL/min, GHSV= 36,000 /h; Plasma condition: 21%O_2/N_2, RH= 50%(25 °C), F= 100 mL/min, GHSV= 36,000 /h, Input Power= 30 W.

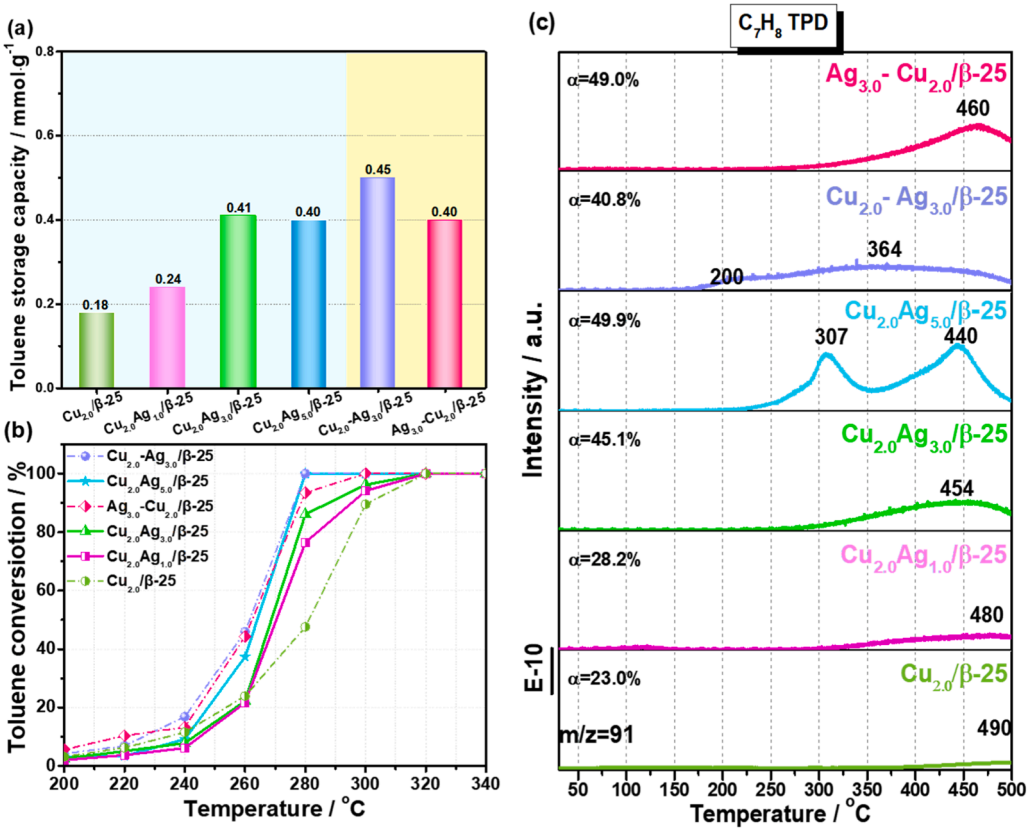

Fig. 9. (a) Toluene storage capacity over series of $Cu_{2.0}Ag_y$/β-25 and Cu&Ag/β-25 catalysts with different loading sequence under humid condition. Storage condition: 25 ppm C_7H_8/21%O_2/N_2, RH= 50% (25 °C), F= 100 mL/min, GHSV= 36,000 /h; (b) The performance of toluene oxidation to CO_2 over series of $Cu_{2.0}Ag_y$/β-25 and Cu&Ag/β-25 catalysts with different loading sequence. Oxidation condition: 25 ppm C_7H_8/21% O_2/N_2, RH= 50% (25 °C), F= 100 mL/min and GHSV = 36,000 /h; (c) Toluene TPD experiments over CuAg supported β zeolites with different Ag content and loading sequence. C_7H_8-TPD condition: N_2, F= 100 mL/min, GHSV= 36,000 /h, 10 °C /min, 30–500 °C; The α represent the proportion of desorption toluene.

oxidation state was maintained during the "storage-in situ oxidation" cycle. While the UV–vis spectra showed some difference, as shown in Fig. S7 (c). For the fresh $Cu_{2.0}Ag_{3.0}$/β-25 sample, much stronger bands due to isolated Cu^{2+} and Ag^+ ions located at the ion-exchange sites of β zeolite, as well as the bands at 270 and 320 nm ascribed to the charged $Ag_n^{\delta+}$ clusters were clearly observed. After reaction, the intensity of these bands declined, accompanied by the enhancement of the band in the visible region, which might result from the aggregated metallic Ag or CuO_x. As can be seen in the TEM images (Fig. S7 (d)), the particle size of CuAg nanoparticles were slightly enlarged but still well-dispersed, being in accordance with the UV–vis results.

6. Discussion

Zeolite materials have been widely explored as absorbents for BTEX removal, which is responsive for H_2O and VOCs competition with various SiO_2/Al_2O_3 ratios [65]. Meanwhile, if the adsorbed BTEX could be directly oxidized into CO_2 (g) and H_2O (g) in-bed, the zeolite could be in-situ regenerated and be available for another adsorption to realize a cycling removal. Thus the applied zeolite should possess the bi-functional abilities to store BTEX at room temperature, and then in-situ oxidize the enriched pollutants during regeneration.

Herein, β zeolite was selected as adsorbent due to the matched channel diameter (6.7 Å) with the kinetic diameter of toluene (5.9 Å), and Cu or/and Ag was introduced to the zeolite acting as active centers for catalytic storage and oxidation (To avoid the confusing, we prefer to name the "chemical adsorption" as a kind of "storage" being characterized with strong interaction and the formation of new bonds) [66–68]. The location and nuclearity of Cu and Ag species in both hydrophilic (SiO_2/Al_2O_3 =25) and hydrophobic (SiO_2/Al_2O_3 =300) β zeolite were compared and identified, which was found to response to toluene and water competition smartly. The bonding strength of toluene on metal sites and zeolite substrate were discriminated. It was revealed that toluene chemically stored on isolated Cu^{2+} or Ag^+ ions located on the cation exchange site of β-zeolite [36,50,69–71]. As revealed by in-situ DRIFTs results, toluene was partially oxidized into benzyl alcohol during room temperature storage. This is reasonable that electron deficient Cu^{2+} or Ag^+ ions are prone to attract the electrons of methyl in toluene and form chemical bonding with metallic exchange sites of zeolite [36,72]. In addition, the charged $Ag_n^{\delta+}$ cluster in the channel of β-zeolite, where the number of nucleation is suggested to be 2–8, showed storage capacity for toluene simultaneously [50]. Owing to the variation in nucleation number, the desorption of toluene over $Ag_n^{\delta+}$ was featured with overlapped and broad desorption between 250–500 °C. Such strong bonding was attributed to the toluene adsorption on the $Ag_n^{\delta+}$ by π-complexes [49,50]. As to the zeolite substrate, BrÖnsted proton sites trapped toluene more tightly than the channel or cage [73,74], which should be related to the charge polarization associated with hydrophilic β zeolite with low SiO_2/Al_2O_3 ratio [65]. On this basis, toluene can be stored (chemically adsorbed) on the metal ions at ion-exchange sites of zeolite (Cu^{2+} and Ag^+), the affinity between toluene and metal ion is strong enough to bind VOCs until reaching the "light-off" temperature for catalytic oxidation, consequently, the toluene could be stored on samples for a long time followed the by oxidizing removal procedure.

For the catalytic oxidation of toluene, nanosized CuO particles and Ag nanoparticles on the outer surface of zeolite show the best activity for toluene oxidation at elevated temperatures. This was evidenced by the fact that best performance was obtained over $Cu_{5.0}$/β-300 and $Ag_{5.0}$/

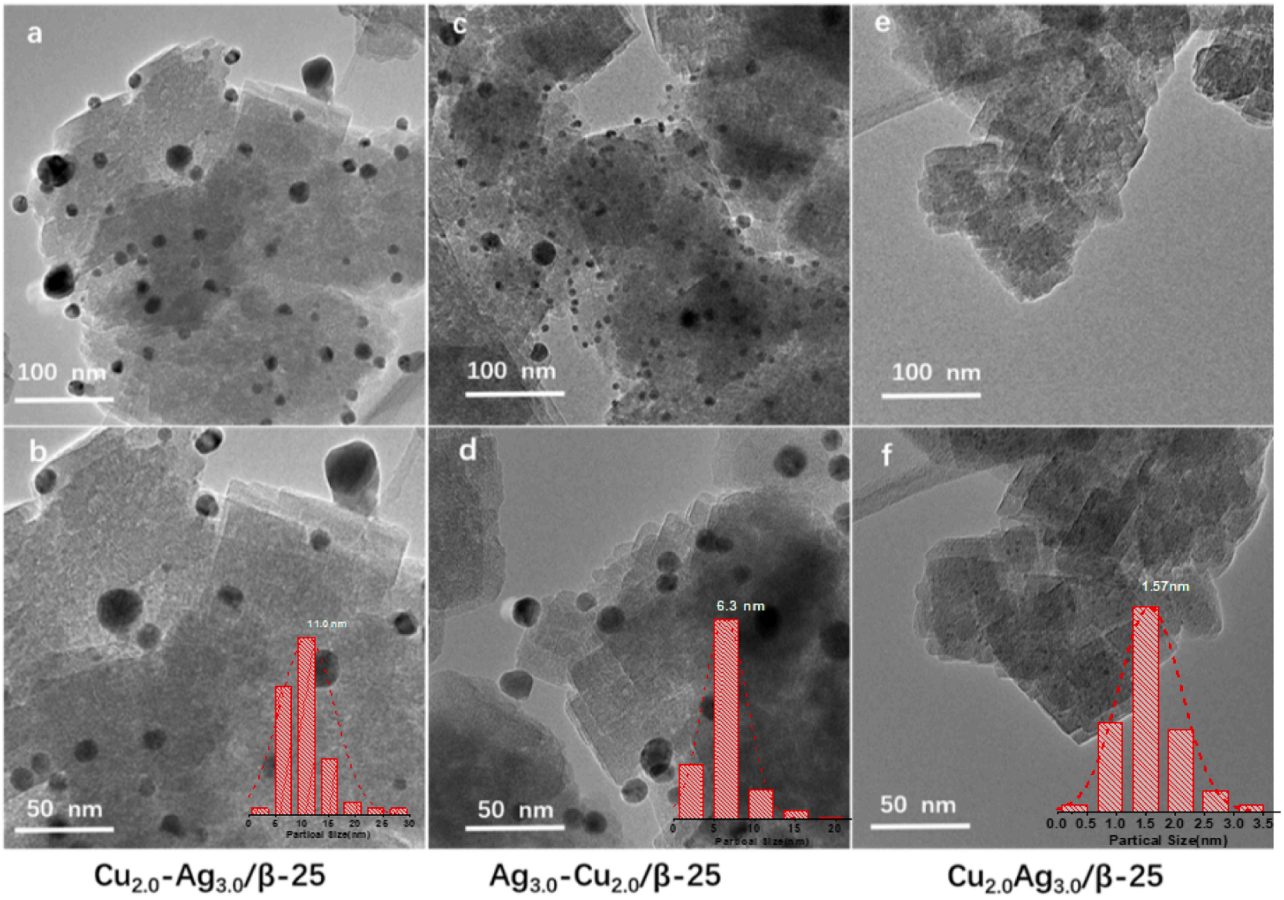

Fig. 10. TEM images of $Cu_{2.0}Ag_{3.0}$/β-25 with different loading sequence (a-b) impregnate copper first and then silver (c-d) impregnate silver first and then copper (e-f) co-impregnation.

β-300 samples respectively, which completely oxidize toluene into CO_2 and H_2O both at 275 °C. As it is recognized that activate of O_2 is the rate-limiting step for toluene catalytic oxidation, thereby it is suggested that nanosized CuO particles and Ag NPs facilitate catalyzing the adsorption and dissociation of O_2, and thereby accelerate the reaction rate apparently [45,75–81].

As to a material employed in the "storage - oxidation" cycle, the storage and oxidation ability for toluene should be balanced considered. The storage capacity is not the only standard to evaluate a material, more importantly, it requires that the oxidation rate for toluene is faster than it's desorption during the regeneration period to ensure that there is no release of adsorbed toluene. Accordingly, stronger bonding between toluene and adsorbents is preferred to leave the temperature window for catalytic oxidation. In the present study, based on the discrimination of the bonding strength of toluene on metal sites (ion-exchange sites, metallic clusters, and aggregated nanoparticles), and zeolite substrate (BrÖnsted sites and channels), a $Cu_{2.0}Ag_{3.0}$/β-25 catalyst was rationally designed by virtue of the collaboration of identified Cu^{2+} and Ag^{+} ions as well Ag clusters for chemical toluene storage, which enable the "storage-thermal oxidation" cycle for toluene removal occurring efficiently. Therefore, by modulating the location of Cu and Ag species in β zeolite, we can enable such smart and responsive materials being available for the toluene "storage- oxidation".

Meanwhile, it is worthy to address that the hydrophilic zeolite with low SiO_2/Al_2O_3 ratio is preferred in this cycled process, which is different with those for general adsorption applications [82]. As shown in the present study that hydrophobic β-300 zeolite do possess much higher storage capacity for toluene in the presence of H_2O (RH=50% (25 °C)), especially when proper amount of Ag was loaded [83]. However, since toluene was physically enriched in the channel of the hydrophobic zeolite, which is easily desorbed below 200 °C (Fig. S2). At this temperature, the catalytic oxidation for toluene has not been started up, which results in the release of stored toluene without oxidation. Alternatively, cold plasma could enable the oxidation taking place at room temperature and fulfill the cycled removal without release of adsorbed toluene. Therefore, an adjustment was made from the balanced consideration between the materials adsorption strength and oxidation ability, either thermal or plasma oxidation was coupled to regenerate the material to execute the cycled removal [22–25,84].

By contrast, hydrophilic zeolite β-25 provides more ion-exchange sites for Cu^{2+} and Ag^{+} ions, which is indispensable for in-situ thermal regeneration. More significantly, the toluene molecules preferentially and selectively adsorbed on these strong bonding sites to minimize the surface energy spontaneously, owing to its chemical reaction in essence. Meanwhile H_2O molecules preferentially take over the zeolite channel due to its hydrophilic property, which is meaningful to avoid the existence of physically adsorbed VOCs, being easily desorbed during regeneration. The important role of water was confirmed by the experiment testing in the dry gas, as shown in Fig. S8. The $Cu_{2.0}$/β-25, $Ag_{5.0}$/β-25 and $Cu_{2.0}Ag_{3.0}$/β-25 catalysts exhibited similar toluene storage capacity in the absence of water, and most stored toluene desorbed below 200 °C, implying toluene was physically enriched in the channel of the β-25 zeolite. Moreover, the release of toluene before oxidation is inevitable due to the weak bonding between toluene and catalyst, which leads to the oxidized conversion of stored C_7H_8 to CO_x far less than 100% (Fig. S8 (c)).

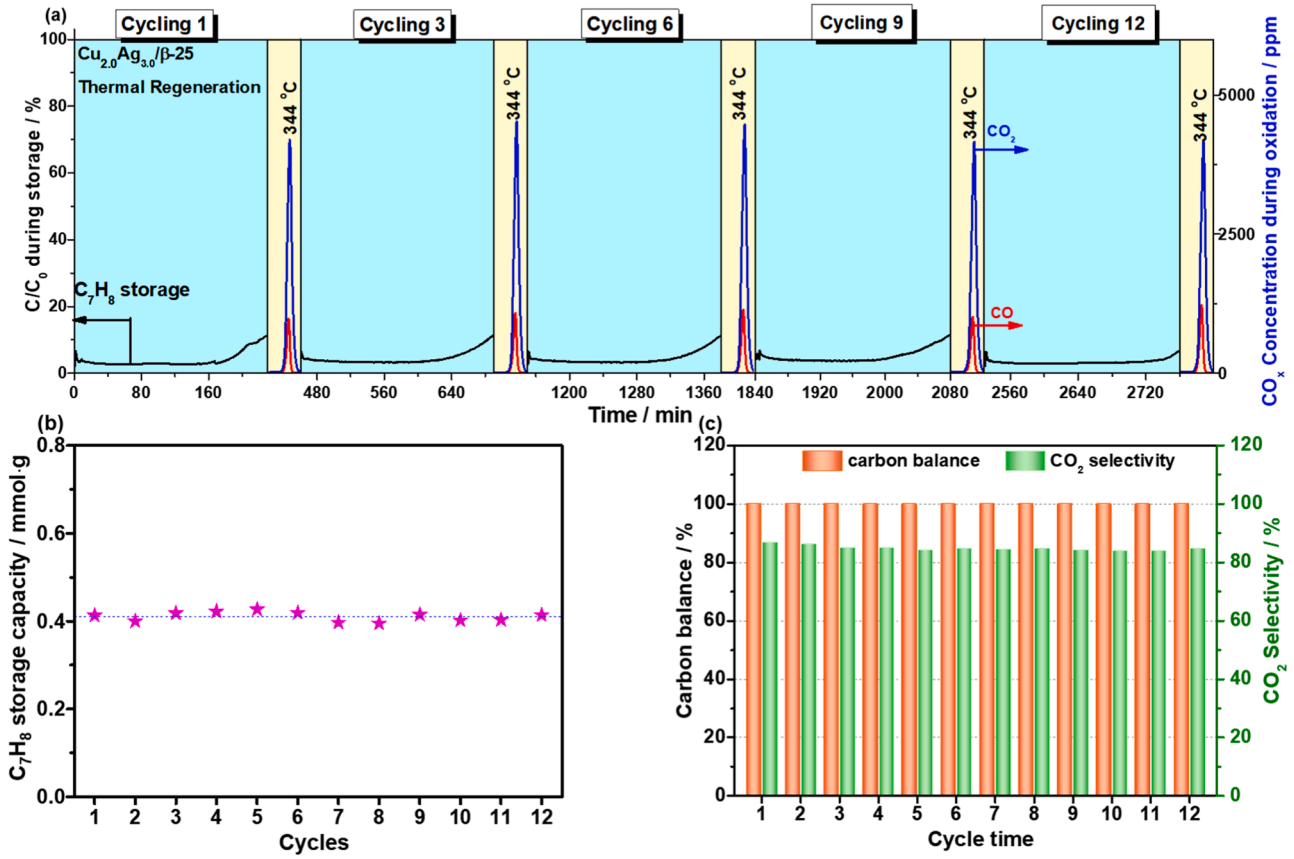

Fig. 11. Toluene breakthrough curve (measured during storage phase) and CO_x concentration (measured during oxidation phase) during twelve consecutive "storage-thermal regeneration" cycles over $Cu_{2.0}Ag_{3.0}$/β-25 zeolite. Storage condition: 25 ppm C_7H_8 /21%O_2/N_2, RH= 50%(25 °C), F= 100 mL/min, GHSV= 36,000 /h; Oxidation condition: 21%O_2/N_2, RH= 50%(25 °C), F= 100 mL/min, GHSV= 36,000 /h, Heating rate= 10 °C/min.

7. Conclusion

Toluene could be smartly and preferentially adsorbed on the metal ion-exchange sites of Cu^{2+} and Ag^{+}, which forms a chemical bonding to storage toluene as benzyl alcohol. Meanwhile H_2O will preferentially take over the zeolite channel for hydrophilic β zeolite, which just prevents the weak storage of toluene in the channel. Over the designed $Cu_{2.0}Ag_{3.0}$/β-25 catalyst, the enhanced storage capacity and trapping strength for toluene enable the in-situ thermal regeneration feasible. On the other hand, if toluene is mostly adsorbed in the channel of hydrophobic β zeolite, it is inevitable for the release of adsorbed toluene during thermal regeneration due to the weak and physical interactions, and a fast oxidation technique of cold plasma was introduced to accelerate the oxidation rate. The study presents a smart process of "Identification of storage sites - Adjusting regeneration approach - Executing the cycle" for toluene removal, which provides a general guidance for BTEX removal.

CRediT authorship contribution statement

Lanlan Zhang: Investigation, Data curation, Writing - Original Draft; Writing - review & editing, Validation. **Zhihui Wang:** Data curation, Methodology, Writing - original draft. **Danyu Liu**: Data curation, Validation. **Zelong Hao:** Data curation, Validation. **Qi Zhao:** Writing - review & editing, **Bingbing Chen:** Writing - review & editing, Supervision, Funding acquisition, **Chuan Shi:** Writing - review & editing, Funding acquisition, Supervision, Project administration.

Declaration of Competing Interest

The authors declare that they have no known competing financial interests or personal relationships that could have appeared to influence the work reported in this paper.

Data availability

No data was used for the research described in the article.

Acknowledgment

The work was supported by the National Natural Science Foundation of China (Nos. 22276023, 21932002), the National Key R&D Program of China (No. 2021YFA1501102), the Fundamental Research Funds for the Central Universities (DUT22ZD212, DUT22LAB602 and DUT22QN207), Liaoning Binhai Laboratory Project (LBLF-202306), the Liaoning Revitalization Talent Program (XLYC2008032), the Scientific Research Fund of Liaoning Provincial Education Department (Grant No. LJKZ0982), the Natural Scientific Fund of Liaoning Province (Grant No. 2023-ES-155). The authors thank Xin Liu from Dalian University of Technology for providing Ddensity functional theory (DFT) calculations.

Appendix A. Supporting information

Supplementary data associated with this article can be found in the online version at doi:10.1016/j.apcatb.2023.123625.

References

[1] U. Poschl, M. Shiraiwa, Chem. Rev. 115 (2015) 4440–4475.
[2] C. He, J. Cheng, X. Zhang, et al., Chem. Rev. 119 (2019) 4471–4568.
[3] L. Xu, C. He, M. Zhu, et al., Catal. Lett. 114 (2007) 202–205.
[4] T. Gelles, A. Krishnamurthy, B. Adebayo, et al., Catal. Today 350 (2020) 3–18.
[5] X. Zhang, B. Gao, A.E. Creamer, et al., J. Hazard. Mater. 338 (2017) 102–123.
[6] Y. Wang, Z. Li, C. Tang, et al., Environ. Sci. Nano 6 (2019) 3113–3122.
[7] C. Yang, G. Miao, Y. Pi, et al., Chem. Eng. J. 370 (2019) 1128–1153.
[8] N. Hoeven, G. Mali, M. Mertens, et al., Micropor. Mesopor. Mater. 288 (2019), 109588.
[9] J. Zhang, X. Xu, S. Zhao, et al., Catal. Today 410 (2023) 56–67.
[10] Y. Chai, W. Dai, G. Wu, et al., Acc. Chem. Res. 54 (2021) 2894–2904.
[11] D. Murindababisha, A. Yusuf, Y. Sun, et al., Int. Environ. Sci. Pollut. Res. 28 (2021) 62030–62060.
[12] H. Liu, N. Li, M. Feng, et al., Environ. Sci. Nano 9 (2022) 1858–1868.
[13] M. Feng, S. Chen, G. Li, et al., Chem. Eng. J. 464 (2023).
[14] B. Chen, L. Wu, B. Wu, et al., ChemCatChem 11 (2019) 3646–3661.
[15] Y. Wang, B. Chen, B. Wu, et al., Catal. Today 297 (2017) 193–200.
[16] Y. Wang, S. Yao, M. Crocker, et al., Catal. Sci. Technol. 5 (2015) 4968–4972.
[17] Y. Wang, C. Dai, B. Chen, et al., Catal. Today 258 (2015) 616–626.
[18] Y. Wang, A. Zhu, B. Chen, et al., Catal. Commun. 36 (2013) 52–57.
[19] C. Shi, B. Chen, X. Li, et al., Chem. Eng. J. 200-202 (2012) 729–737.
[20] A. Urbutis, S. Kitrys, Open Chem. 12 (2014) 492–501.
[21] C. Shi, Y. Wang, A. Zhu, et al., Catal. Commun. 28 (2012) 18–22.
[22] M. Qu, Z. Cheng, Z. Sun, et al., Process. Saf. Environ. 153 (2021) 139–158.
[23] S. Li, X. Dang, X. Yu, et al., Chem. Eng. J. 388 (2020), 124275.
[24] W. Chung, D. Mei, X. Tu, et al., Catal. Rev. 61 (2018) 270–331.
[25] O. Karatum, M.A. Deshusses, Chem. Eng. J. 294 (2016) 308–315.
[26] G. Kresse, J. Hafner, Phys. Rev. B 49 (1994) 14251–14269.
[27] G. Kresse, J. Non-Cryst. Solids 193 (1995) 222–229.
[28] J.P. Perdew, K. Burke, M. Ernzerhof, Phys. Rev. Lett. 77 (1996) 3865–3868.
[29] S. Grimme, S. Ehrlich, L. Goerigk, J. Comput. Chem. 32 (2011) 1456–1465.
[30] S. Grimme, J. Antony, S. Ehrlich, et al., J. Chem. Phys. 132 (2010) 19.
[31] S.L. Dudarev, G.A. Botton, S.Y. Savrasov, et al., Phys. Rev. B 57 (1998) 1505–1509.
[32] G. Kresse, D. Joubert, Phys. Rev. B 59 (1999) 1758–1775.
[33] M. Gajdos, A. Eichler, J. Hafner, J. Phys. Condens. Matter 16 (2004) 1141–1164.
[34] D.H. Mei, O.A. Lercher, J. Phys. Chem. C 123 (2019) 25255–25266.
[35] A.K. Mishra, A. Roldan, N.H. de Leeuw, J. Phys. Chem. C 120 (2016) 2198–2214.
[36] Y. Du, G. Xiao, Z. Guo, et al., Sci. Total. Environ. 833 (2022), 155288.
[37] Q. Zhao, B. Chen, B. Zou, et al., Catal. Sci. Technol. 11 (2021) 646–655.
[38] J. Guo, W. Yang, Y. Zhang, et al., Catal. Commun. 135 (2020), 105751.
[39] N. Wilken, R. Nedyalkova, K. Kamasamudram, et al., Top. Catal. 56 (2013) 317–322.
[40] C. Liang, X. Li, Z. Qu, et al., Appl. Surf. Sci. 258 (2012) 3738–3743.
[41] X. Feng, Y. Cao, L. Lan, et al., Chem. Eng. J. 302 (2016) 697–706.
[42] H. Wang, R. Xu, Y. Jin, et al., Catal. Today 327 (2019) 295–307.
[43] B. Pereda-Ayo, U. De La Torre, M.J. Illán-Gómez, et al., Appl. Catal. B 147 (2014) 420–428.
[44] J. Zhou, J. Catal. 225 (2004) 128–137.
[45] T. Yin, X. Meng, S. Wang, et al., Sep. Purif. Technol. 280 (2022), 119634.
[46] S. Xiong, N. Huang, Y. Peng, et al., J. Hazard. Mater. 415 (2021), 125637.
[47] P. Sazama, J. Moravkova, S. Sklenak, et al., ACS Catal. 10 (2020) 3984–4002.
[48] A.J. Maira, J.M. Coronado, V. Augugliaro, et al., J. Catal. 202 (2001) 413–420.
[49] L. Heredia, E. Colombo, P. Quaino, et al., Top. Catal. 65 (2022) 934–943.
[50] V. Temerev, A. Vedyagin, T. Afonasenko, et al., React. Kinet. Catal. Lett. 119 (2016) 629–640.
[51] W. Ma, X.A. Dong, Y. Wang, et al., Appl. Surf. Sci. 578 (2022), 152002.
[52] J. Li, X.A. Dong, G. Zhang, et al., J. Mater. Chem. A 7 (2019) 3366–3374.
[53] Y. He, H. Ji, Chin. J. Catal. 31 (2010) 171–175.
[54] L. Kundakovic, M. Flytzani-Stephanopoulos, Appl. Catal. A 183 (1999) 35–51.
[55] S. Dzwigaj, Y. Millot, J.-M. Krafft, et al., J. Phys. Chem. C 117 (2013) 12552–12559.
[56] C. Shi, M. Cheng, Z. Qu, et al., J. Mater. Chem. A 235 (2005) 35–43.
[57] D. Chen, J. Shi, Y. Yao, et al., React. Kinet. Catal. Lett. 127 (2019) 315–329.
[58] S. Aspromonte, E. Miró, A. Boix, Adsorption 18 (2011) 1–12.
[59] J. Li, H. Na, X. Zeng, et al., Appl. Surf. Sci. 311 (2014) 690–696.
[60] M. Netto, J. Oliveira, N. Salau, et al., J. Environ. Chem. Eng. 9 (2021), 104960.
[61] J. Cui, R. Yeasmin, Y. Shao, et al., Ind. Eng. Chem. Res. 59 (2019) 751–762.
[62] X. Zhou, G. Miao, G. Xu, et al., Chem. Eng. J. (450 () (2022).
[63] H. Yang, C. Ma, X. Zhang, et al., ACS Catal. 8 (2018) 1248–1258.
[64] W. Zhang, G. Li, H. Yin, et al., Environ. Sci. Nano 9 (2022) 81–104.
[65] M. Kraus, U. Trommler, F. Holzer, et al., Chem. Eng. J. 351 (2018) 356–363.
[66] A. Rokicińska, M. Drozdek, B. Dudek, et al., Appl. Catal. B 212 (2017) 59–67.
[67] Y. Li, L. Li, J. Yu, Chem 3 (2017) 928–949.
[68] B. Ilić, S.G. Wettstein, Micropor. Mesopor. Mater. 239 (2017) 221–234.
[69] N. Viswanadham, S.K. Saxena, Aa.H. Al-Muhtaseb, Mater. Today Chem. 3 (2017) 37–48.
[70] N. Blanch-Raga, A.E. Palomares, J. Martínez-Triguero, et al., Appl. Catal. B 187 (2016) 90–97.
[71] W. Wang, H. Wang, T. Zhu, et al., J. Hazard. Mater. 292 (2015) 70–78.
[72] X. Hou, H. Li, P. He, et al., J. Phys. Chem. A 119 (2015) 11199–11207.
[73] E. Grifoni, G. Piccini, J.A. Lercher, et al., Nat. Commun. 12 (2021), 2630.
[74] A. Palčić, V. Valtchev, Appl. Catal. A 606 (2020), 117795.
[75] M. Ibrahim, M. Labaki, A. Ponchel, et al., ChemCatChem 15 (2022).
[76] W. Xu, X. Chen, J. Chen, et al., J. Hazard. Mater. 403 (2021), 123869.
[77] K. Bhargavi, D. Ray, P. Chawdhury, et al., Catalysts 12 (2022) 421.
[78] N. Mikheeva, V. Zaikovskii, Y. Larichev, et al., Mater. Today Chem. 21 (2021), 100530.
[79] X. Ma, M. Xiao, X. Yang, et al., J. Colloid Interface Sci. 594 (2021) 882–890.
[80] Y. Qin, Y. Wang, J. Li, et al., Surf. Interfaces 21 (2020), 100657.
[81] C. Qin, X. Huang, X. Dang, et al., Chemosphere 162 (2016) 125–130.
[82] S. Baek, J. Kim, S. Ihm, Catal. Today 93-95 (2004) 575–581.
[83] B. Bal'zhinimaev, E. Paukshtis, A. Toktarev, et al., Micropor. Mesopor. Mater. 277 (2019) 70–77.
[84] M. Zheng, D. Yu, L. Duan, et al., Catal. Commun. 100 (2017) 187–190.